The Vertical Structure of Tropospheric Water Vapor: Comparing Radiative and Ocean-Driven Climate Changes

BRIAN E. J. ROSE AND M. CAMERON RENCURREL

Department of Atmospheric and Environmental Sciences, University at Albany, State University of New York, Albany, New York

(Manuscript received 14 July 2015, in final form 11 March 2016)

ABSTRACT

Changes in column-integrated water vapor (Q) in response to increased CO_2 and ocean heat uptake (OHU) are investigated in slab-ocean aquaplanet simulations. The simulations span a wide range of warming and moistening patterns due to the spatial structures of the imposed OHU. Fractional changes in Q per degree of surface warming range from 0% to 20% K^{-1} locally and from 3.6% to 11% K^{-1} globally. A new diagnostic technique decomposes these changes into relative humidity (RH), surface temperature, and lapse rate contributions. Single-column calculations demonstrate substantial departures from apparent (surface temperature based) Clausius–Clapeyron (CC) scaling due to lapse rates changes; a moist-adiabatic column with fixed, uniform RH exceeds the CC rate by 2.5% K^{-1}. The RH contribution is very small in most simulations. The various Q scalings are thus all consistent CC, but result from different patterns of polar amplification and lapse rate change. Lapse rates are sensitive to location and magnitude of OHU, with implications for Q under transient climate change. CO_2 with subpolar (tropical) OHU results in higher (lower) Q scalings than CO_2 alone. The weakest Q scaling (and largest RH effects) is found for increased poleward ocean heat transport, which causes strongly polar-amplified warming and near-zero tropical temperature change. Despite weak RH changes and fidelity to the CC relation, Q is expected to vary widely on different time scales in nature due to sensitivity of lapse rates to OHU along with the nonlinearity of the diagnostics.

1. Introduction

Water vapor is a central player in the climate system. The hydrological cycle is tightly coupled to atmospheric radiation, energetics, and dynamics. A robust understanding of the processes controlling atmospheric water vapor, therefore, must underlie any theory of climate.

This paper is concerned with understanding the constraints on the atmospheric water vapor budget under various equilibrium and transient climate change scenarios. We quantify the water vapor content using the depth-integrated precipitable water Q (in $kg\,m^{-2}$), which is the mass-weighted column integral of specific humidity q:

$$Q = \int_0^{p_0} q \frac{dp}{g}, \tag{1}$$

where p_0 is the surface pressure. We seek to compare and contrast the effects on Q of radiative forcing from greenhouse gases with changes in net sea surface heat flux associated with ocean heat uptake and transport.

It is widely recognized that Q scales nonlinearly with temperature under climate change. The primary reason is the roughly exponential nature of the Clausius–Clapeyron (CC) relation governing saturation vapor pressure e_s:

$$\frac{1}{e_s}\frac{de_s}{dT} = \frac{L}{R_v T^2} \equiv \alpha(T), \tag{2}$$

where L is the appropriate latent heat and R_v is the gas constant for water vapor. Equation (2) states that fractional changes in saturation vapor pressure occur at a roughly constant rate, with $\alpha \approx 7\%\ K^{-1}$ at typical lower-tropospheric temperatures [though as we will detail below, $\alpha(T)$ is a weakly decreasing function of temperature]. The specific humidity is the mass ratio of water vapor to total moist air (see appendix A). It follows that q should change by approximately the same fractional

Corresponding author address: Brian E. J. Rose, Atmospheric and Environmental Sciences, University at Albany, State University of New York, 1400 Washington Ave., Albany, NY 12222.
E-mail: brose@albany.edu

DOI: 10.1175/JCLI-D-15-0482.1

rate α so long as fractional changes in relative humidity are small.

What does this imply about changes in Q? Should we expect that fractional changes $(1/Q)(dQ/dT_s)$ to be closely determined by the CC rate $\alpha(T_s)$ at the surface temperature T_s? Even in the simple limit of fixed relative humidity (RH), the answer depends on the spatial distribution of both temperature and water vapor, and on temperature lapse rate changes in each column (i.e., differences in warming rates aloft relative to the surface). Careful quantification of these issues is a major goal of this paper.

In a seminal study, Held and Soden (2006) plotted fractional changes in global mean precipitable water $\overline{Q}$ from transient coupled global warming simulations from the CMIP3 archive, and found a robust scaling $(1/\overline{Q})(d\overline{Q}/d\overline{T_s}) \approx 7.5\%\ \mathrm{K}^{-1}$ (overbars denote global averages). This is often cited as evidence for CC scaling of atmospheric water vapor. However, there are a number of subtleties to this argument (O'Gorman and Muller 2010). Recent studies have examined a variety of different global and local diagnostics for fractional changes in Q in simulations of past and future climate change, and found a diversity of different results. We will review these results below. However, because some of this diversity is associated with methodological differences in the spatial averaging of Q, it is helpful to begin with careful definitions for each diagnostic and their mathematical relationships. This will bring greater clarity to our review of previous work, and introduce notation used throughout this paper.

a. Spatial averaging of column water vapor diagnostics

Because both water vapor and temperature vary spatially in the atmosphere, there is no unique way to express the fractional rate of change in Q in a changing climate. (All the following have units of $\%\ \mathrm{K}^{-1}$.) First, a purely local diagnostic:

$$\delta Q_{\mathrm{local}} \equiv \frac{1}{Q}\frac{dQ}{dT_s} = \frac{d}{dT_s}\log(Q) \tag{3}$$

(i.e., the local fractional rate of change of Q per degree local surface temperature change).

The same local rate can also be rescaled to the global mean temperature change:

$$\delta Q_{\mathrm{hybrid}} \equiv \frac{1}{Q}\frac{dQ}{d\overline{T_s}}. \tag{4}$$

Finally, a purely global metric is the fractional change in global mean Q per degree global mean temperature change:

$$\delta Q_{\mathrm{global}} \equiv \frac{1}{\overline{Q}}\frac{d\overline{Q}}{d\overline{T_s}}. \tag{5}$$

It is important to recognize that these three diagnostics all measure different things, and will not be equal given any significant spatial structure to the warming pattern—both vertically and horizontally (Boos 2012). For later reference, we will write down mathematical relationships between each diagnostic. Introducing the local temperature amplification factor

$$\tau = \frac{\delta T_s}{\overline{\delta T_s}}. \tag{6}$$

Then we can write

$$\delta Q_{\mathrm{hybrid}} = \tau \delta Q_{\mathrm{local}}, \tag{7}$$

which can be averaged globally to give a meaningful measure (denoted here $\overline{\delta Q_{\mathrm{hybrid}}}$) of how the average *local* column water vapor changes per degree global warming.

The global and local diagnostic are then related through

$$\delta Q_{\mathrm{global}} = \overline{\left(\frac{Q}{\overline{Q}}\tau\delta Q_{\mathrm{local}}\right)}, \tag{8}$$

that is, the global average is strongly weighted toward the tropics where the ratio $Q/\overline{Q}$ is large.

b. Recent work on scaling of column water vapor

Held and Soden (2006) focused on $\delta Q_{\mathrm{global}}$. It is not entirely clear why this should be the quantity of primary interest. It is not related in any simple way to either the hydrological cycle or the water vapor feedback, both of which might be argued to be have a closer connection to $\delta Q_{\mathrm{local}}$. However $\delta Q_{\mathrm{global}}$ is widely reported in the literature so it behooves us to understand the constraints on this quantity and its connection to local measures under different climate change scenarios. Note that Q is not the only possible metric for atmospheric water vapor and its scaling under climate change. Some authors have instead (or in addition) used near-surface specific humidity to measure agreement with the CC relation (e.g., O'Gorman and Muller 2010).

Lorenz and DeWeaver (2007) plotted a measure equivalent to $\delta Q_{\mathrm{local}}$ at several extratropical latitudes in an ensemble of CMIP3 global warming simulations, which they compared to $\alpha(T)$ measured at the 850-hPa air temperature. They found scalings about $1\%\ \mathrm{K}^{-1}$ below the CC rate at 40°N/S and about $1\%\ \mathrm{K}^{-1}$ above the CC rate at 55°S. They tentatively ascribed these differences to changes in relative humidity, but did not analyze the effects of changing lapse rates.

O'Gorman and Muller (2010) calculated the zonal mean δQ_{local} as a function of latitude for an ensemble of CMIP3 global warming simulations, and also compared these values to δQ_{hybrid}. They tabulated global mean values of δQ_{global}. They found that both δQ_{local} and δQ_{hybrid} vary strongly with latitude, anywhere from 6% to 12% K^{-1}. They also show the largest δQ_{local} (12% K^{-1}) occurs over the Southern Ocean where *transient heat uptake* is occurring and surface temperatures are depressed in the coupled models. This suggests that the vertical structure of the warming and the nonlocal effects of mixing by the atmosphere must be taken into account in order to understand the actual scaling of water vapor under the influence of ocean heat uptake (OHU). It also suggests that methodological care is required when comparing water vapor scalings between models and scenarios.

O'Gorman and Muller (2010) also calculated a CC scaling using simulated temperature changes and assuming fixed RH. The difference between these and the actual δQ_{local} values is attributed to changes in RH under global warming. They found slight RH decreases in subtropics and midlatitudes, and slight increases in the deep tropics, giving deviations of order 1% K^{-1} between the actual δQ and the CC rate. They are careful to point out that the vertical structure of temperature change (along with the temperature dependence of the CC rate) are important factors in deviations of δQ_{local} from the canonical 7.5% K^{-1}. However, they do not attempt to separate the effect of changes in lapse rate.

Boos (2012) used simulations from the Paleoclimate Modelling Intercomparison Project phase 2 (PMIP2) archive to study changes in the hydrological cycle associated with the warming from the Last Glacial Maximum (LGM) to preindustrial conditions. He found $\delta Q_{\text{global}} \approx 5\%\ \text{K}^{-1}$, apparently substantially smaller than the expected CC rate. On the other hand, the global mean of the local fractional changes ($\overline{\delta Q_{\text{hybrid}}}$ in our notation) were larger, ranging between 6.5% and 8.0% K^{-1}. Boos (2012) attributes this difference to the strong polar amplification of the LGM to modern warming. Relative to future global warming scenarios, a greater fraction of the global mean warming occurs near the poles where precipitable water content is relatively small (in our notation, τ is smaller near the equator where $Q/\overline{Q}$ is large). Thus, δQ_{global} is suppressed despite local scaling of water vapor consistent the CC relation. Changes in RH were found to play a secondary role, but a relative moistening of the tropical lower troposphere from LGM to preindustrial contributed to an order 1% K^{-1} increase in δQ_{local} beyond the expected value for fixed RH across the tropics.

Following this same line of reasoning, Back et al. (2013) compared δQ_{global} in "rapid" versus "slow" global warming phases in a long historical run of a coupled GCM. Rapid here means transient changes in which significant OHU is still taking place. They found substantially weaker than expected changes for slow (i.e., equilibrium) warming, about 4.2% K^{-1}. The authors suggest that δQ_{global} is quite sensitive to the spatial structure of the surface warming (i.e., to the factor τ in our notation). The term τ itself is known to depend strongly on the nature and spatial structure of the climate forcing, and in particular, is sensitive to the spatial structure of OHU for transient climate change (e.g., Rose et al. 2014).

Taken together, these previous results all suggest that δQ_{global} can span a large range of values for a multitude of reasons, and is not a particularly useful measure of actual deviations from CC scaling of column water vapor. Furthermore, while the vertical structure of the temperature change has been acknowledged as a potentially important factor determining changes in Q by several authors (O'Gorman and Muller 2010; Boos 2012; Back et al. 2013), this has not been carefully quantified. In this study we are particularly interested in the effects of OHU during transient climate change on the vertical structure of temperature and water vapor changes.

c. *Goals of this study*

The goals of the present work are twofold. First, we seek to understand clearly the implications of the CC relation and RH changes for the scaling of Q in environments where temperature lapse rates may be changing. Second, we study the effects of OHU on the scaling of Q from both a local and global perspective. Following Rose et al. (2014) we compare pure (equilibrium) CO_2-driven warming with scenarios driven by prescribed OHU in a slab ocean GCM, sampling a range of different climate responses mimicking various equilibrium and transient climate change scenarios. We use an idealized aquaplanet model setup, enabling a thorough and unambiguous decomposition of the changes in Q to surface temperature, lapse rate, and RH changes.

We will show that the model produces a wide range of different Q scalings under different forcing scenarios, and furthermore that these arise almost entirely from differences in polar amplification and lapse rate responses, as opposed to significant deviations from fixed relative humidity. In this paper we adopt a local column perspective on Q, taking the patterns of temperature change in response to each forcing as "given" by the numerical model. Since midlatitude eddies play a key role in setting extratropical lapse rates (e.g., Stone 1978) and these effects are sensitive to the moisture content of

the eddies (e.g., Frierson 2008), causal mechanisms linking a particular climate forcing to a particular change in Q are complex. We do attempt to present such a comprehensive theory here.

The rest of this paper is laid out as follows. In section 2 we take a brief look at the observed vertical distribution of specific humidity, and present some illustrative theoretical calculations of δQ_{local} under simple assumptions about the lapse rate. We then develop the decomposition of δQ_{local} into surface temperature, lapse rate, and RH contributions, which is used as a diagnostic framework for our GCM simulations. Section 3 introduces the GCM simulations and the idealized forcings, and the effects of different forcing on the spatial structure of temperature change. We then present an analysis of δQ_{local} associated with each forcing pattern, including its detailed vertical structure, and how these project on global diagnostics $\overline{\delta Q_{\text{hybrid}}}$ and δQ_{global}. We present a discussion and our conclusions in section 4.

2. Observational and theoretical considerations

a. *Observed vertical distribution of tropospheric water vapor*

To further motivate our interest in the vertical structure of water vapor changes, we take a brief look at observations. The question at hand is, what proportion of the observed column water vapor is actually in the free troposphere above the planetary boundary layer? This is plotted by latitude and season in Fig. 1. The data source is the long-term climatology of the NCEP–DOE Reanalysis 2 (Kanamitsu et al. 2002). Climatological specific humidity was computed from air temperature and relative humidity data, and then vertically integrated to obtain the fraction of the total Q occurring above 800 hPa. This diagnostic was then averaged zonally and by season.

Figure 1 shows that about 40% of the total water vapor is above 800 hPa. This fraction is a bit smaller in the subtropical dry regions, and larger in the high latitudes where a temperature inversion is frequently observed. Given that a nontrivial amount of water vapor is above the planetary boundary layer, it follows that water vapor may be sensitive to the vertical structure of climate change.

b. *Effects of lapse rate changes in idealized single-column calculations*

Here we present some simple single-column calculations of δQ_{local} that reveal the potential importance of lapse rate changes on the water vapor budget. For these calculations we assume that RH is fixed and *vertically uniform* in the column (ignoring the vertical structure of RH is not very realistic but greatly simplifies these idealized calculations). For such a column we can then

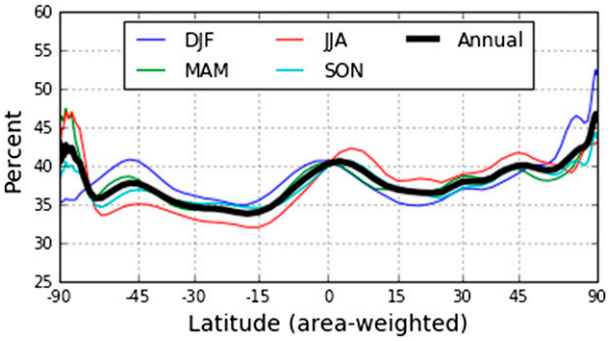

FIG. 1. Fraction of observed total column water vapor above 800 hPa, from long-term mean data in the NCEP–DOE Reanalysis 2.

replace q by its saturation value q_{sat} at every level when calculating fractional changes. We calculate δQ_{local} as a function of surface temperature for a small differential warming, under three different assumptions about the lapse rate $\Gamma = -dT/dz$:

1) Temperature decreases uniformly with height, $\Gamma = \text{constant} = 6.5\,\text{K km}^{-1}$, with the same warming rate at every level.
2) Γ is vertically uniform ($6.5\,\text{K km}^{-1}$) but decreases with warming at a fractional rate $-1.5\%\,\text{K}^{-1}$ (warming rate is greater aloft than at the surface).
3) Γ is moist adiabatic everywhere (thus warming also increases upward).

The results are plotted in Fig. 2 and compared against the CC rate $\alpha(T_s)$. We calculate Q numerically, approximating the differential as a finite difference over a small temperature increase. We use formulas from Bolton (1980) for e_s and from Pierrehumbert (2010) for the temperature dependence of the latent heat of vaporization and the slope of the moist pseudoadiabat.

First, Fig. 2 shows that α varies between about $6\%\,\text{K}^{-1}$ at tropical temperatures to about $10\%\,\text{K}^{-1}$ at cold polar temperatures. For a fixed, uniform lapse rate and RH, δQ_{local} is about $0.5\%\,\text{K}^{-1}$ larger than α due to the presence of significant water vapor at colder temperatures above the surface. A decrease in the lapse rate with warming implies an increase in δQ_{local} by about the same amount as the fractional change in Γ (here $1.5\%\,\text{K}^{-1}$), and thus a rate substantially larger than α. It is thus possible for δQ_{local} to exceed $\alpha(T_s)$ wherever there are large fractional changes in the lapse rate. We will refer to these changes as *apparent super-CC rates*. They are of course all exactly consistent with the CC relation because we have computed them by assuming fixed relative humidity. Interestingly, the apparent super-CC scaling of δQ_{local} is even larger for a moist-adiabatic column (at least for surface temperatures above the freezing point); δQ_{local} exceeds α by a temperature-dependent amount

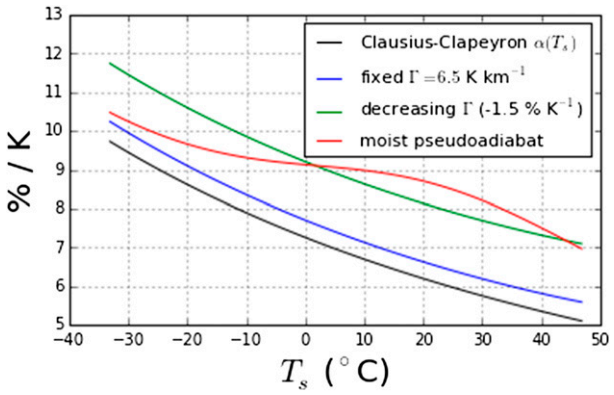

FIG. 2. Fractional rates of change of precipitable water, $(1/Q)(dQ/dT_s)$ as a function of surface temperature T_s computed for columns with fixed relative humidity, under three different assumptions about the lapse rate Γ. (blue) Γ is constant and held fixed at 6.5 K km^{-1} (column warms uniformly). (green) Γ decreases at a fractional rate of 1.5% K^{-1}. (red) Moist-adiabatic column $-$ Γ is the pseudoadabatic lapse rate. (black) The Clausius–Clapeyron rate $\alpha(T_s)$.

that peaks at a surface temperature of 23.4°C, and is very close to 2.5% K^{-1} over the whole range of relevant tropical temperatures.

c. *Quantifying contributions of relative humidity and lapse rate changes to column water vapor*

Since the water vapor content of tropospheric air is typically well below saturation, we will define CC scaling of Q in terms of changes (or lack thereof) in relative humidity, denoted as r. We can write

$$q(p) = r(p) q_{\mathrm{sat}}(T, p), \tag{9}$$

where q_{sat} is the saturation specific humidity at the ambient temperature and pressure [obtained by setting $e = e_s(T)$ in (A1)].[1]

It follows that, for small differential temperature changes at any point, we can write

$$\frac{1}{q}\frac{dq}{dT} = \frac{1}{q_{\mathrm{sat}}}\frac{dq_{\mathrm{sat}}}{dT} + \frac{1}{r}\frac{dr}{dT}, \tag{10}$$

which expresses fractional changes in q in terms of two additive contributions: the rate of change of saturation specific humidity at the ambient conditions (dictated by CC), and the fractional change in relative humidity. Expressing in terms of differential changes in *surface* temperature we can write

$$\frac{1}{q}\frac{dq}{dT_s} = \frac{1}{q_{\mathrm{sat}}}\frac{dq_{\mathrm{sat}}}{dT}\frac{dT}{dT_s} + \frac{1}{r}\frac{dr}{dT_s}. \tag{11}$$

Taking the vertical integral, it then follows that the fractional change in column water vapor can be decomposed as

$$\delta Q_{\mathrm{local}} = \left\langle \alpha \frac{dT}{dT_s} \right\rangle + \left\langle \frac{1}{r}\frac{dr}{dT_s} \right\rangle, \tag{12}$$

where for shorthand we write $(1/q_{\mathrm{sat}})(dq_{\mathrm{sat}}/dT) = \alpha$ (though in detail this term actually differs from the CC rate for saturation vapor pressure by a small pressure-dependent correction), and the angle braces denote a humidity-weighted vertical average:

$$\langle A(p) \rangle \equiv \frac{\int_0^{p_0} A(p) q(p)\, dp}{\int_0^{p_0} q(p)\, dp} \tag{13}$$

for any quantity $A(p)$.

The fractional rate of change in Q can thus be unambiguously decomposed into separate temperature and relative humidity effects. The relative humidity contribution is proportional to its fractional change, weighted by the reference state specific humidity.

As is traditional in climate feedback analysis, we now separate temperature changes into two contributions: a vertically uniform component equal to the surface temperature change, and a vertically varying residual associated with changes in the lapse rate.

In the absence of lapse rate changes $dT/dT_s = 1$ everywhere, and the CC contribution to fractional changes in Q would be simply $\langle \alpha(T) \rangle$ [where $T = T(p)$ is the vertically varying temperature of the control climate]. We can then define the contribution to changes in Q associated with lapse rate changes as a residual $\langle \alpha(T)(dT/dT_s) \rangle - \langle \alpha(T) \rangle$.

We thus arrive at a three-term decomposition:

$$\delta Q_{\mathrm{local}} = \delta Q_{T_s} + \delta Q_{\mathrm{lapse}} + \delta Q_{\mathrm{RH}} \tag{14}$$

with the terms defined as

$$\delta Q_{T_s} = \langle \alpha(T) \rangle, \tag{15a}$$

$$\delta Q_{\mathrm{lapse}} = \left\langle \alpha(T) \frac{dT}{dT_s} \right\rangle - \langle \alpha(T) \rangle, \tag{15b}$$

$$\delta Q_{\mathrm{RH}} = \left\langle \frac{1}{r}\frac{dr}{dT_s} \right\rangle. \tag{15c}$$

[1] The RH diagnostic reported by the CAM model used in this study is defined in terms of specific humidity, so (9) is exact. If RH is alternately defined in terms of either vapor pressure or mixing ratio, there will be a small correction to these formulas depending on the temperature profile of the control climate. The corrections are negligible in the dilute limit $e/p \ll 1$, which characterizes Earth's climate.

We will use this decomposition to analyze the changes in Q simulated in a suite of GCM experiments.

d. The importance of fractional changes in lapse rate

The idealized numerical calculations in Fig. 2 shows that an imposed fractional change in lapse rate, $(1/\Gamma)(d\Gamma/dT_s) = -1.5\%\,\mathrm{K}^{-1}$ increases $\delta Q_{\mathrm{local}}$ by about the same amount. This result can be demonstrated analytically to a good approximation. Details are given in appendix A. For a column with a vertically uniform lapse rate and relative humidity, there is a closed form for the vertical integral of specific humidity in (A10) that shows that the dependence of Q on the lapse rate is Γ^{-1}. It follows that fractional changes in Q can be written approximately as

$$\delta Q_{\mathrm{local}} \approx \frac{L}{R_v T_s^2} - \frac{1}{\Gamma}\frac{d\Gamma}{dT_s} + \frac{1}{r}\frac{dr}{dT_s}. \tag{16}$$

In this approximation, the uniform temperature and lapse rate contributions to changes in Q are the following:

$$\delta Q_{T_s} \approx \alpha(T_s) \tag{17a}$$

$$\delta Q_{\mathrm{lapse}} \approx -\frac{1}{\Gamma}\frac{d\Gamma}{dT_s}. \tag{17b}$$

3. Water vapor changes in idealized GCM simulations

a. Model description and control simulation

In this section we analyze the changes in column water vapor simulated in an aquaplanet GCM subjected to a variety of idealized forcings. The model is NCAR's CAM4 (Neale et al. 2013) (the atmospheric component of the coupled CCSM4) coupled to an idealized slab ocean aquaplanet surface with prognostic sea surface temperature (SST). The model uses a finite-volume dynamical core at 2.0° × 2.5° horizontal resolution and 26 vertical levels. The model setup is identical to that described by Rose et al. (2014), and follows closely earlier proposed benchmarks for aquaplanet simulations (Lee et al. 2008; Neale and Hoskins 2000). Perpetual equinox insolation (zero obliquity) is prescribed with solar constant $1365\,\mathrm{W\,m^{-2}}$. Mixed layer depth is 10 m. Sea surface albedo is fixed at 0.1. Reference greenhouse gas inventories are 348 ppmv CO_2, 1650 ppbv CH_4, and 306 ppbv N_2O (all other greenhouse gases set to zero). Ozone has a prescribed steady, symmetric distribution (Blackburn and Hoskins 2013). Sea ice is omitted but SST below freezing is permitted (no surface albedo feedback). Each simulation is integrated at least 30 years, and climatologies are computed over the last 20 years.

Time-invariant prescribed sources and sinks of energy in the ocean mixed layer temperature equation (so-called q fluxes) are used to represent ocean heat uptake (OHU) and transport (OHT). Our control simulation sets the q flux to zero everywhere, implying a climate with zero OHT. We compare this control climate to perturbation climates with increased CO_2 and as well as imposed q fluxes that represent idealized OHU and OHT patterns, which we describe in detail below. Following Rose et al. (2014) we compare the responses to OHU patterns localized in the high latitudes versus the tropics, both alone and in combination with increased CO_2. We also analyze the climatic perturbation associated with an idealized increase in OHT (Rose and Ferreira 2013).

Figure 3 shows several relevant aspects of the control climate (all results are shown as zonal and time averages over the period of quasi-equilibrium). The surface temperature varies smoothly between 305 K at the equator and about 233 K at the poles and is symmetric about the equator. The global mean value is $\overline{T_s} = 288.6\,\mathrm{K}$. The global mean precipitable water is $\overline{Q} = 32.1\,\mathrm{kg\,m^{-2}}$; the normalized distribution $Q/\overline{Q}$ ranges from 2.65 at the equator to 0.07 at the poles (Fig. 3b).

From (15a), the expected local scaling of column water vapor in the absence of changes in RH and lapse rate is $\delta Q_{T_s} = \langle \alpha(T) \rangle$, which is a property of the reference climate only and independent of the mechanism forcing a particular climate change. This is plotted in Fig. 3c for our control simulation. We computed the humidity-weighted vertical integral of $\alpha = (1/q_{\mathrm{sat}})(dq_{\mathrm{sat}}/dT)$ numerically from zonally averaged temperature data at each latitude. Saturation specific humidity and its derivative were computed with the same numerical routines used in the CAM4 GCM code, which includes a linear interpolation between saturation with respect to water at 0°C and saturation with respect to ice at −20°C (appendix B gives some further details along with a brief sensitivity study with different implementations of the CC relation). The term $\langle \alpha(T) \rangle$ exceeds $\alpha(T_s)$ by at least $0.5\%\,\mathrm{K}^{-1}$ at all latitudes due to the presence of significant water vapor aloft at colder temperatures above the surface. There is a local maximum in the difference at the equator associated with the higher RH aloft within the ITCZ region relative to the dry subtropics. The term $\langle \alpha(T) \rangle$ reaches values greater than $10\%\,\mathrm{K}^{-1}$ at high latitudes.

b. Idealized forcings

We subject our GCM to four different climate forcings, plotted in Fig. 4a. The first is a doubling of atmospheric CO_2 from 348 to 696 ppmv. The radiative forcing due to CO_2 doubling is $3.8\,\mathrm{W\,m^{-2}}$ globally; its spatial structure is shown by the black curve in Fig. 4a. This was estimated by the regression method (Crook et al. 2011;

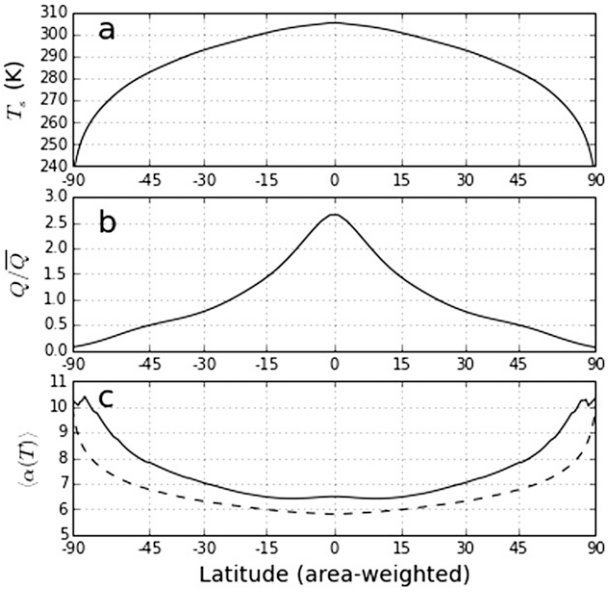

FIG. 3. Climatology of the perpetual equinox aquaplanet control simulation. (a) Zonal, time mean surface temperature T_s in K. (b) Column water vapor normalized by the global mean, $Q/\overline{Q}$. (c) The uniform temperature contribution to local column water vapor changes, $\langle\alpha(T)\rangle$ (solid line) compared to the Clausius–Clapeyron rate $\alpha(T_s)$ computed at the local surface temperature (in % K^{-1}).

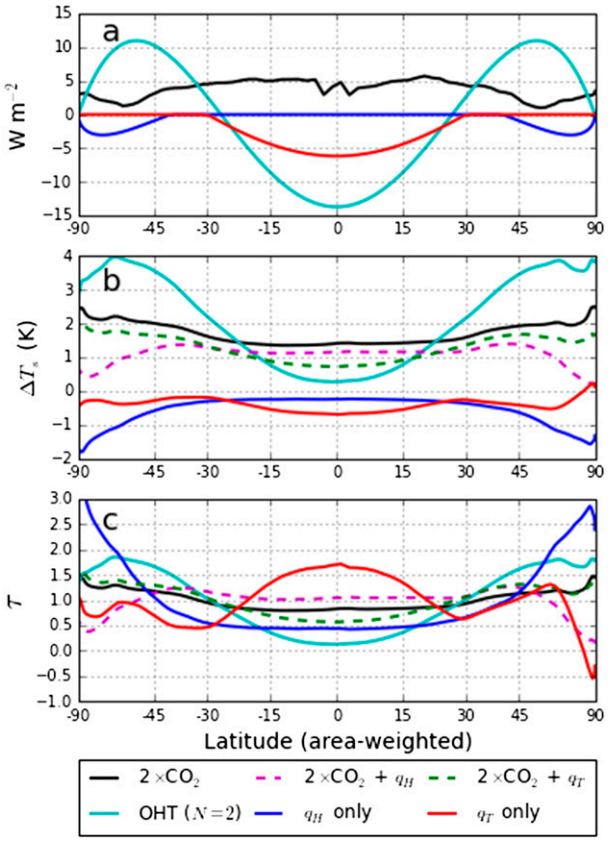

FIG. 4. Forcings and equilibrium temperature responses in the aquaplanet GCM simulations. (a) TOA radiative forcing (for 2 × CO_2) and imposed q fluxes (for OHT, q_H and q_T). The CO_2 radiative forcing was estimated by the regression method from a transient simulation as described by Rose et al. (2014). (b) Equilibrium surface temperature anomalies from control climate. (c) The normalized local temperature amplification factor τ.

Gregory et al. 2004) in a slowly warming transient simulation with a 200-m ocean mixed layer, as described by Rose et al. (2014). The curve is not smooth due to the noisiness inherent in the regression method. It is shown here for comparison with the other forcings, but is not used in any of the diagnostics to follow.

The other three forcings are time-invariant heat sources/sinks applied to the ocean mixed layer. Following Rose et al. (2014), we study the effects of OHU during transient climate change as a quasi-equilibrium problem (taking advantage of the separation of time scales between the atmosphere/surface ocean and deep ocean mixing processes), by specifying steady heat sinks in the shallow ocean mixed layer and simulating the equilibrium climate response to that heat sink. We define two different spatial patterns of OHU, one localized to the subpolar latitudes (denoted q_H) and another localized to the tropics (q_T).[2] These are also plotted (in W m^{-2}) in Fig. 4a, where a negative value indicates a heat sink at that latitude. Both patterns are symmetric about the equator; formulas are given in Rose et al. (2014). These heat sinks are applied both in combination with 2 × CO_2 (to mimic transient global warming), and in isolation. See Rose et al. (2014) for further motivation and description of these experiments. Global mean heat sinks are $\overline{q_T} = 2\,\mathrm{W\,m^{-2}}$ and $\overline{q_H} = 0.7\,\mathrm{W\,m^{-2}}$. In contrast with Rose et al. (2014) we reduced the amplitude of q_H in order to ensure that the simulated surface temperature response in the combined forcing experiment 2 × CO_2 + q_H is greater than zero at all latitudes.

Finally we analyze the climate change associated with a 1-PW increase in OHT. This is imposed as a specified ocean heat sink across the tropics and a heat source in the mid- to high latitudes, peaking at 50°N/S (cyan curve in Fig. 4a). The implied northward OHT is a smoothly varying function of latitude antisymmetric about the equator (no cross-equatorial heat transport), using the formula from Rose and Ferreira (2013): OHT $\propto \sin\phi\cos^{2N}\phi$ with meridional-scale parameter $N = 2$ and ϕ is latitude in radians. The global mean heat source/sink in this case is zero; the forcing just imposes a meridional redistribution of energy in the slab ocean.

[2] We use this notation for consistency with Rose et al. (2014). Here q_H, q_T refer to energy fluxes imposed on the slab ocean, and should not be confused with specific humidity.

c. Temperature and circulation responses

Figure 4b shows the equilibrium surface temperature change (anomaly from the control climate) associated with each forcing. Figure 4c shows these same temperature changes normalized by their respective global mean values to give the temperature amplification factor τ. The vertical structure of the warming/cooling patterns are contoured in Fig. 5, along with changes in the overturning circulation.

Doubling CO_2 in our ice-free aquaplanet produces 1.7-K global mean surface warming, with a modestly polar-amplified pattern (Figs. 4b,c), and the expected warming maximum in the tropical upper troposphere (Fig. 5). The circulation changes indicate a weakening and widening of the Hadley cells (Fig. 5). Comparing this pure $2 \times CO_2$ response to the combined CO_2 plus OHU experiments gives idealized analogies to equilibrium versus transient global warming, which have been shown to produce different water vapor scalings (Back et al. 2013). Considering the $2 \times CO_2 + q_H$ case, high-latitude OHU suppresses the greenhouse warming at all latitudes, but the effect is strongest near the poles under the direct effect of the local heat sink. The resulting surface warming pattern is roughly uniform (about 1.2 K) equatorward of 50° but near zero at high latitudes, in analogy with the delayed warming of the Southern Ocean in transient coupled GCM simulations. Significantly for this discussion, Fig. 5 also shows that this "transient" case has a stronger vertical gradient in the warming of the lower troposphere (less warming below 800 hPa) compared with the "equilibrium" $2 \times CO_2$ case. The effect of q_H in isolation is a strongly polar-amplified and surface-trapped cooling pattern. The temperature and circulation anomalies associated with $2 \times CO_2$ and OHU are very nearly additive (Rose et al. 2014).

As discussed extensively by Rose et al. (2014), the efficacy (Winton et al. 2010) of tropical OHU is much weaker than high-latitude OHU. Though the amplitude of the forcing for q_T is 3 times larger than q_H, the surface temperature response is actually weaker in the global mean (0.4 K cooling for q_T vs 0.5 K for q_H). Tropical heat uptake produces a modest surface cooling at almost all latitudes,[3] with maximum cooling at the equator. However, Fig. 5 shows that the cooling pattern for q_T is amplified aloft; the upper troposphere cools substantially across the tropics and subtropics. The combined forcing case $2 \times CO_2 + q_T$ (which we speculate might be analogous to greenhouse warming under sustained La Niña or hiatus conditions) in fact produces the most spatially uniform warming pattern (in latitude and pressure) of our whole ensemble.

A 1-PW increase in OHT produces a global warming of 2.1 K in our aquaplanet. This is a new result not yet reported elsewhere, though it is qualitatively consistent with Rose and Ferreira (2013) who used a substantially less sophisticated atmospheric GCM, and with other recent work on the climatic impact of OHT (Herweijer et al. 2005; Barreiro et al. 2011; Koll and Abbot 2013). It is remarkable that a globally conservative redistribution of energy in the ocean mixed layer yields a global warming, and suggests significant spatial heterogeneity of climate feedback processes (even in the absence of surface snow and ice at high latitudes, which are not represented in our model). The warming has a unique spatial pattern; it is near zero in the deep tropics (both at the surface and throughout the column), and greater than 3 K across the mid- to high latitudes. This warming is largest at the surface in the regions of direct heating, but extends deeply through the midlatitude troposphere. It is accompanied by the most pronounced circulation changes in our ensemble, including substantial weakening of both the tropical Hadley cells and midlatitude Ferrel cells. A detailed study of the atmospheric circulation response to changes in OHT is in preparation by the authors and will be presented elsewhere.

Collectively our ensemble of six perturbation experiments span a wide range of different spatial patterns of temperature change, ranging from strongly polar amplified to equatorially amplified, with a diversity of different vertical structures. Our central question is, how do these different warming patterns translate into different changes in column water vapor, and what role do non-CC processes (i.e., changes in relative humidity) play in these changes?

d. Changes in column water vapor

Figure 6 shows the local fractional changes in precipitable water associated with each forcing. δQ_{local} is plotted as a function of latitude (white solid lines) and compared to $\delta Q_{T_s} = \langle \alpha(T) \rangle$ (white dashed lines, identical to Fig. 3c). These plots are superimposed on contour plots showing cross sections of the local contributions to the vertical integrals. The contoured quantity is proportional to $dq/dT_s/Q$. We multiply by a constant factor $M \times 100\%$ where $M = \int_0^{p_0} dp/g \approx 10^4\,\text{kg m}^{-2}$ is the column mass, so the field actually has units of $\%\,\text{K}^{-1}\,(10^4\,\text{kg m}^{-2})^{-1}$. This

[3] The exception is a small warming at the North Pole for q_T. This asymmetry is most likely associated with locally enhanced variability of the polar climate and would not be found in a longer time average or an ensemble mean of several simulations; however we note that ΔT_s crosses zero at about 68°N in q_T, which will introduce some numerical noise into our water vapor diagnostics to be presented in the next section.

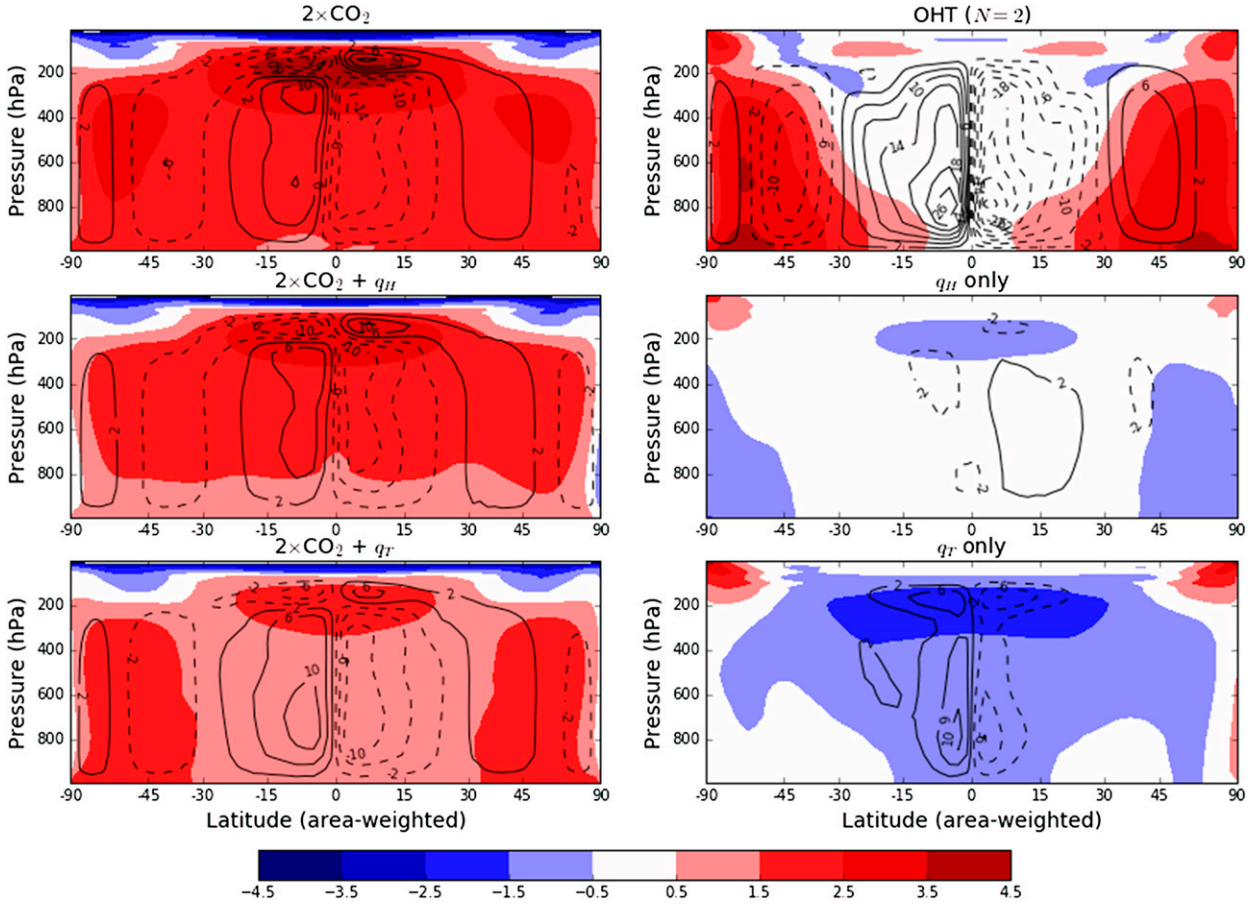

FIG. 5. Vertical structure of temperature and circulation changes at equilibrium in the aquaplanet GCM simulations. Air temperature changes are shown in colors with 1-K contour intervals. Overturning circulation changes are shown as contours of anomalous mean meridional mass transport (black, contour interval is 4×10^9 kg s^{-1}).

ensures that a vertically uniform field would have the same numerical value at every level as the mass-weighted column integral δQ_{local} (in % K^{-1}). The contours thus indicate where in the column the dominant water vapor changes are occurring. Differential rates of change are estimated from the simulated finite-amplitude changes through the following formula:

$$\frac{dq}{dT_s} \approx \frac{q}{\Delta T_s} \log\left(1 + \frac{\Delta q}{q}\right), \tag{18}$$

where q is the control specific humidity, and Δq, ΔT_s are the simulated changes. This correction is appropriate for hydrological quantities that increase roughly exponentially with temperature (O'Gorman and Muller 2010). Global averages are summarized in Table 1 for the local diagnostic $\overline{\delta Q_{\text{hybrid}}}$ and Table 2 for the global diagnostic δQ_{global} (the tables also include decompositions of the Q changes into temperature and RH changes that will be discussed below).

We first note some points of agreement and disagreement with previous results. We find $\delta Q_{\text{global}} = 7.4\%$ K^{-1} for 2 × CO_2 (Table 2), which appears to agree very closely with Held and Soden (2006). However, those results were for transient global warming simulations, for which our 2 × CO_2 + q_H case (high-latitude OHU) is the best analog. We find substantially larger $\delta Q_{\text{global}} = 9.2\%$ K^{-1} in this case. This is consistent with the main finding of Back et al. (2013) in which δQ_{global} tends to be greater for transient than for equilibrium warming. Our values are greater overall (Back et al. found only 4.2% K^{-1} for equilibrium warming). We suppose that the absence of relatively dry land surfaces in our aquaplanet simulations leads to overall larger changes in column water vapor than expected for Earth.

Comparing 2 × CO_2 with 2 × CO_2 + q_H in Fig. 6, we find that δQ_{local} differs primarily over the subpolar heat uptake regions, where δQ_{local} reaches values as high as 20% K^{-1} (far exceeding the local CC rate for vertically uniform warming). This is consistent with O'Gorman

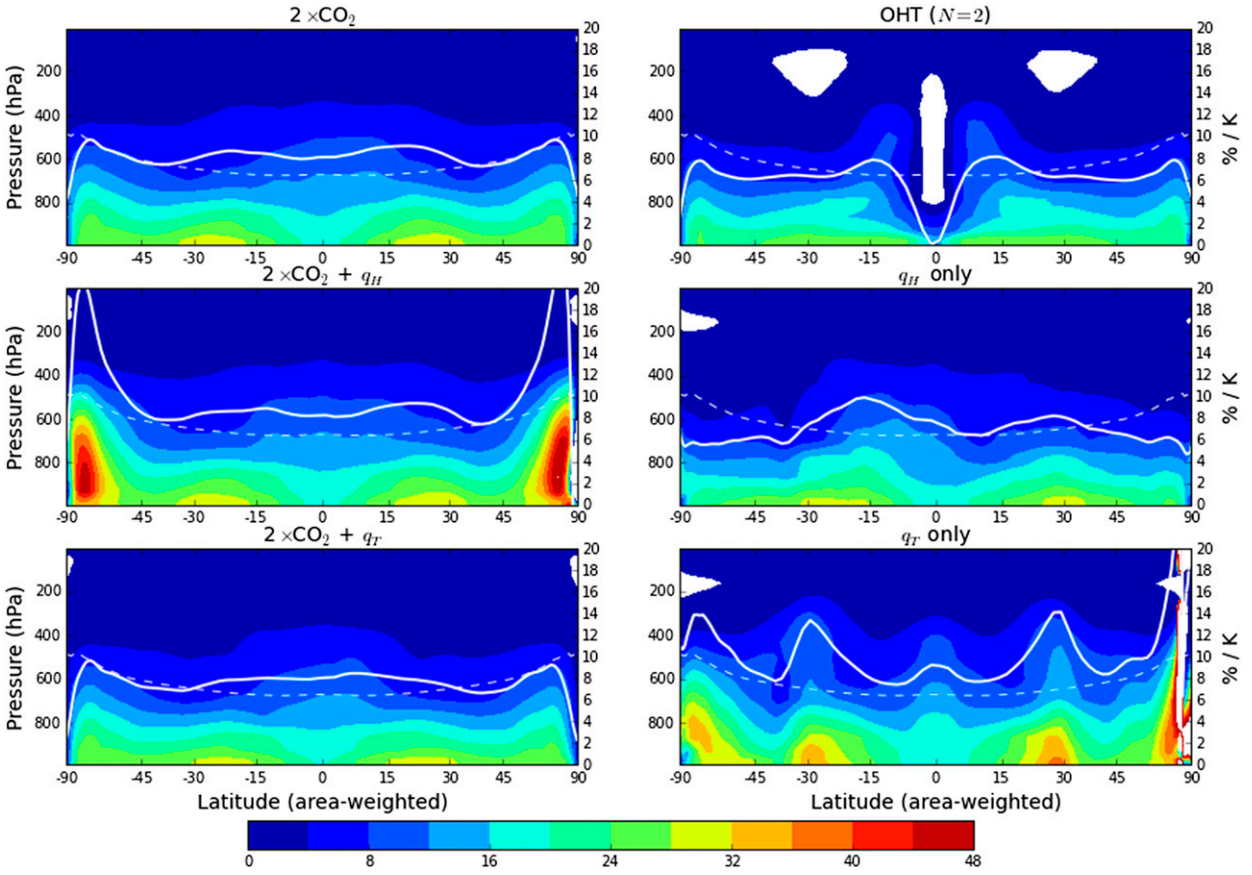

FIG. 6. Differential fractional changes in column water vapor. The white solid lines are the local fractional change δQ_{local}; dashed lines are the uniform warming contributions $\langle \alpha(T) \rangle$ computed from the control climate as shown in Fig. 3. Units are % K^{-1}, with the axis on the right-hand side of each panel. Also shown in color contours: vertical cross sections of $\delta q/(QT_s)^{-1}$, which integrate vertically to give δQ_{local}. The contours thus show contributions from different vertical levels to the fractional changes in Q. Units are % K^{-1} $(10^4\ \text{kg m}^{-2})^{-1}$ (a vertically uniform field would thus have the same numerical value as the column integral). All quantities are expressed as differential rates using (18) [correcting for finite-amplitude temperature changes, following O'Gorman and Muller (2010)].

and Muller (2010) who also found elevated values of δQ_{local} over the Southern Ocean in transient coupled simulations. Figure 6 shows that this is associated with specific humidity changes extending deeply over the entire lower troposphere. A novel feature of our analysis is the explicit decomposition of this difference into lapse rate and RH changes, to follow in the next section.

The results discussed in the previous two paragraphs are specific to *high-latitude* OHU. We find that transient warming in the presence of *tropical* OHU exhibits rather different scalings for column water vapor. Figure 6 shows that δQ_{local} is in fact nearly identical for $2 \times CO_2$ and $2 \times CO_2 + q_T$. On the other hand, the small decrease in the proportion of global mean temperature change occurring in the tropics for $2 \times CO_2 + q_T$ (i.e., the quantity τ plotted in Fig. 4c) leads to substantially smaller global mean scalings in this case (Tables 1 and 2).

It is interesting to note that the fractional changes in precipitable water under combined radiative plus OHU forcing, unlike the temperature changes themselves, are not at all additive. Figure 6 shows that δQ_{local} is suppressed far below the local CC rate throughout the mid- to high latitudes in the q_H-only case, while for the q_T-only case this diagnostic is larger at most latitudes, with peaks of 13%–14% K^{-1} near 30°N/S where the surface temperature response is weakest (Figs. 4b,c). The strongly polar (equatorially) amplified temperature change for q_H (q_T) produces smaller (larger) global mean scalings for Q than any of the CO_2-driven cases. These differences are found in the global mean of the local changes (Table 1) but are even more evident in δQ_{global} (Table 2), with $\delta Q_{\text{global}} = 4.4\%\ K^{-1}$ for q_H and $11.0\%\ K^{-1}$ for q_T.

Water vapor changes associated with increased OHT are also quite distinct from all our other cases. Figure 6 shows that δQ_{local} is actually zero at the equator, with negative specific humidity anomalies throughout a deep layer in the convective deep tropics. The term δQ_{local} is

TABLE 1. Global mean values of the *local* fractional change in precipitable water $\overline{\delta Q_{\text{hybrid}}}$ for our six different types of climate forcing, and its decomposition into contributions due to surface warming, lapse rate changes, and relative humidity changes. The residual is the difference between the total change in Q and the sum of the three partial contributions. (All values in % K^{-1}, expressed as differential rates.)

	$2 \times CO_2$	$2 \times CO_2 + q_H$	$2 \times CO_2 + q_T$	q_H only	q_T only	OHT ($N = 2$)
Total	8.2	9.3	7.6	6.5	9.5	6.5
Uniform	7.7	7.3	7.7	8.3	7.2	8.1
Lapse rate	0.9	2.2	0.2	−1.5	3.1	−1.7
Relative humidity	−0.1	−0.2	−0.2	0.0	−0.7	0.3
Residual	−0.2	0.0	−0.2	−0.4	−0.0	−0.2

also suppressed well below the local CC rate through the mid- to high latitudes. Together these effects add up to the weakest overall global scalings of our entire ensemble: δQ_{global} is only 3.6% K^{-1} in this case (Table 2). It is evident that climate changes driven by surface heat fluxes are not equivalent to those driven by CO_2 in terms of the spatial structure of temperature and water vapor changes.

e. *Real versus apparent non-Clausius–Clapeyron water vapor changes*

Here we use the decomposition in (14) to quantify the relative importance of actual non-CC scaling (δQ_{RH}) versus apparent non-CC scaling associated with lapse rate changes (δQ_{lapse}) and vertically uniform warming (δQ_{T_s}) in our GCM ensemble. In Fig. 7 δQ_{RH} is plotted versus latitude for each experiment (black solid lines in lower panels). As in Fig. 6 we also contour the vertical structure of contributions to the humidity-weighted vertical integral (black contours in upper panels). We compute the local differential change of RH as $\Delta \log(r)/\Delta T_s$ at each grid point (using the time- and zonal-mean RH fields generated by the GCM), eliminating the need to correct for finite-amplitude temperature changes (Boos 2012). On the same graphs we also plot δQ_{lapse} (green solid lines) and its vertical structure (color contours; the same contour intervals as for δQ_{RH} contributions). The global mean values for each term in the decomposition are also listed in Tables 1 and 2.

First, a brief comment about the hemispheric asymmetries in Figs. 6 and 7. Because the model setup and forcings are symmetric about the equator, any asymmetries are due to internal model variability. Despite the relatively long simulation time (diagnostics are computed from 20-yr averages after model spinup), some asymmetries remain, which are amplified in the noisier diagnostics in Figs. 6 and 7. We interpret these asymmetries as rough measures of the uncertainty in these diagnostics.

Our analysis shows that RH changes play a very minor role in total column water vapor changes in most, but not all, cases, with δQ_{RH} typically smaller than 0.5% K^{-1} in absolute value at all latitudes, and with the global means substantially smaller than that. The implication is that the large range of different local and global scalings of Q found in our ensemble are, for the most part, all consistent with the CC relation, which projects differently onto the very different spatial structures of temperature change under the different forcing scenarios.

There are two interesting exceptions to the above generalization: the tropical heat uptake case q_T and the increased OHT case both exhibit important RH changes. It is perhaps not a coincidence that both cases also involve substantial net heat fluxes through the tropical sea surface—although we do not pursue a dynamical explanation for this result here. The term δQ_{RH} is negative across the subtropics in q_T, indicating increased RH associated with the cooling and net flux of heat into the tropical ocean. These RH anomalies (weighted by the background specific humidity) have deep structures centered around 600 hPa and extending throughout the subtropical troposphere. The RH

TABLE 2. As in Table 1, but for the *global* fractional change in precipitable water δQ_{global}. (All values in % K^{-1}, expressed as differential rates.)

	$2 \times CO_2$	$2 \times CO_2 + q_H$	$2 \times CO_2 + q_T$	q_H only	q_T only	OHT ($N = 2$)
Total	7.4	9.2	6.2	4.4	11.0	3.6
Uniform	6.1	7.2	5.6	4.4	8.4	4.2
Lapse rate	1.4	2.1	0.8	0.1	3.6	−1.0
Relative humidity	0.0	−0.0	−0.1	0.1	−0.8	0.4
Residual	−0.1	−0.1	−0.1	−0.1	−0.2	−0.0

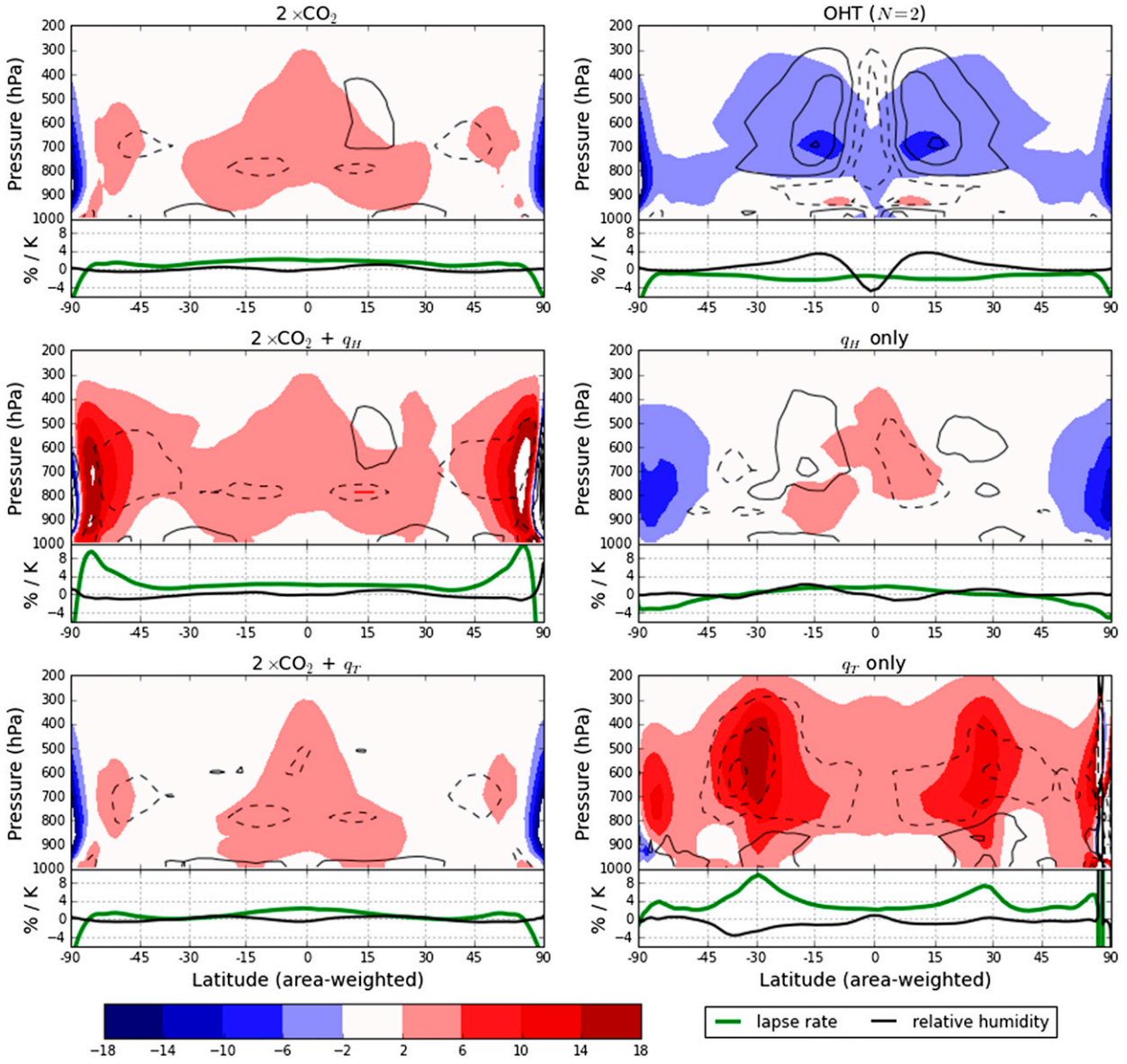

FIG. 7. Contributions of lapse rate and relative humidity to fractional rate of rate of column water vapor. Line plots show column integrals δQ_{lapse} and δQ_{RH} in $\%\,\text{K}^{-1}$. Contours show local contributions to the humidity-weighted vertical integral in $\%\,\text{K}^{-1}$ $(10^4\,\text{kg m}^{-2})^{-1}$ (same units as in Fig. 6) with a contour interval of 4. Colors show lapse rate contribution; black contours show relative humidity contribution. Negative RH contours are dashed. The green line plots are thus the column integral of the color contours; black line plots are column integrals of the black contours.

contribution to δQ_{global} is $-0.8\%\,\text{K}^{-1}$ for q_T (Table 2), the largest magnitude in our ensemble.

Enhanced OHT is associated with a distinctive tripole pattern straddling the equator, consistent with the substantial slowdown of the Hadley circulation shown in Fig. 5. There is deep and broad relative moistening across the subtropics centered at 15°N/S, and relative drying of the entire equatorial troposphere, as well as throughout the tropical boundary layer below 850 hPa. This pattern is associated with local extremes in δQ_{RH} as large as $\pm 4\%\,\text{K}^{-1}$, but which are damped out to only $+0.4\%\,\text{K}^{-1}$ in the global mean (Table 2).

As noted previously, δQ_{T_s} depends only on the reference climate and so is identical in all experiments, ranging from $6.5\%\,\text{K}^{-1}$ in the deep tropics to about $10\%\,\text{K}^{-1}$ near the poles (dashed white lines in Fig. 6). Because of the different surface warming patterns, however, this

term projects differently onto the global mean diagnostics in each case. The uniform warming contribution to δQ_{global} (i.e., the scaling of column water vapor expected on the basis of the reference climate and the surface temperature anomalies only) ranges from 4.2% K^{-1} (OHT) to 8.4% K^{-1} (q_T). These results are qualitatively consistent with the arguments put forward by Back et al. (2013): the weakest (strongest) scaling occurs for climate changes with the greatest (least) polar amplification. However, the uniform term systematically underestimates the differences in δQ_{global} across our ensemble. Those cases with the weakest (largest) uniform term *also* have the smallest (largest) lapse rate term (Table 2).

To illustrate this point in more detail we again draw attention to the comparison between the "equilibrium" $2 \times CO_2$ and the "transient" $2 \times CO_2 + q_H$ cases. The actual difference in δQ_{global} is 1.8% K^{-1} as discussed above. Surface temperature changes alone only account for 1.1% K^{-1} of the difference. The remaining 0.7% K^{-1} comes from differences in δQ_{lapse}. Figure 7 shows that δQ_{lapse} is locally very large (near 10% K^{-1}) in the subpolar heat uptake regions in $2 \times CO_2 + q_H$. This is primarily due to the strong local suppression of surface warming in the heat uptake regions, while both the temperature and moisture fields tend to be smoothed out aloft by atmospheric transport. However, we also note that the surface warming is suppressed at all latitudes in the "transient" case, not just in the subpolar heat uptake regions (Figs. 4b and 5), indicating a global dynamical response to the localized heat uptake. Consequently, δQ_{lapse} is positive everywhere equatorward of the heat uptake regions as well (Fig. 7). The difference in the vertical structure of the warming between the transient and equilibrium greenhouse cases is a key factor in the different scalings of Q. This is true whether we adopt the local (Table 1) or global (Table 2) perspective.

There are also several examples in Fig. 7 of locally compensating changes in RH and lapse rate (indicating smaller absolute changes in q than would be predicted from local temperature changes and the CC relation). In the enhanced OHT case, the relative moistening across the subtropics is accompanied by a negative δQ_{lapse} contribution (more warming near the surface than aloft, which can be seen in Fig. 5). Because δQ_{lapse} is negative everywhere away from the poles in this case, it dominates the RH term in the global diagnostics. The tropical heat uptake case q_T features locally large δQ_{lapse} near 30° (as high as 8% K^{-1}) where surface temperature change is very weak but there is significant cooling aloft (Fig. 5). The temperature change and RH change push the total Q in opposite directions, but the lapse rate contribution is substantially larger.

Collectively, Fig. 7 and Tables 1 and 2 indicate that, with a few interesting exceptions, deviations from fixed RH are insignificant contributions in the budget of column water vapor changes. On the other hand, the vertical structure of temperature changes varies widely depending on the nature of the climate forcing in our simulations, and these variations in turn lead to a diversity of different scalings for Q. Changes in lapse rate cannot be ignored in either the local or global perspectives.

Finally we draw attention to the differences between the local and global perspectives, comparing $\overline{\delta Q_{\text{hybrid}}}$ (Table 1) and δQ_{global} (Table 2). Most of the differences are less than 1% K^{-1}, but a few are much larger. We mentioned above that high-latitude heat uptake (q_H) and increased OHT both yield very low values of δQ_{global} (4.4% and 3.6% K^{-1}, respectively), which is dominated by the small uniform δQ_{T_s} contribution. Both of these cases feature small tropical temperature change (τ is small across the low latitudes, Fig. 4c), so the product $\tau Q/\overline{Q}$ weighting the global average in (8) is small. In other words, δQ_{global} is small because the climate changes are strongly polar amplified in these two experiments. Interestingly, the uniform contribution to the local diagnostic $\overline{\delta Q_{\text{hybrid}}}$ is actually *largest* in these same two cases (8.3% and 8.1% K^{-1}, respectively). This result can again be attributed to polar amplification, but in the local perspective it is the larger CC rate at cold polar temperatures that dominates the global mean when weighted by τ in (7). Whether strongly polar-amplified climate change should produce large or small values for the scaling of Q depends very much on whether we adopt the global or local perspective. On the other hand, neither δQ_{global} nor $\overline{\delta Q_{\text{hybrid}}}$ gives much indication of genuine deviation from CC scaling.

4. Discussion and conclusions

Held and Soden (2006) showed that fractional rates of change of integrated global mean precipitable water $\overline{Q}$ (the diagnostic we call δQ_{global}) were consistently near 7.5% K^{-1} in coupled next-century simulations, a rate that would seem to be predicted by the CC relation at representative lower-tropospheric temperatures and fixed relative humidity. On the other hand, more recent work (see our review in section 1b) has shown a diversity of different results for the scaling of Q in equilibrium and transient climate simulations, even in the absence of substantial changes in RH.

Two separate issues have confounded these comparisons. One is the effect of spatial averaging; the same climate change can yield rather different scalings depending on whether Q is averaged before or after calculating fractional rates of change. The second is the

role of the spatial structure of the climate change in question, which can also strongly affect the calculated scalings of Q even in the absence of significant RH changes. Transient climate changes can be understood as a combined response to radiative forcing and ocean heat uptake, which exerts a profound effect on the spatial structure of the warming (Rose et al. 2014). We have sought some clarity on these issues by computing careful budget decompositions for changes in Q in a series of aquaplanet GCM simulations with simple idealized forcing mechanisms that sample a wide range of different climate responses. Previous authors have drawn attention to the importance of polar amplification of surface temperature changes on the scaling of Q (O'Gorman and Muller 2010; Boos 2012; Back et al. 2013). We have extended this perspective to investigate the explicit role of lapse rate changes, and separate these temperature effects as cleanly as possible from actual non-CC scaling associated with changes in relative humidity.

Our analysis hinges on the decomposition in (14) of local fractional changes in Q into contributions associated with vertical uniform warming, lapse rate change, and relative humidity changes. We demonstrated that the relative humidity contribution is equivalent to the vertical integral of fractional changes in RH, weighted by the background specific humidity. We also showed that, for an idealized column with uniform relative humidity, surface temperature T_s and lapse rate Γ, the lapse rate contribution to fractional changes in Q is approximately $-[(1/\Gamma)(d\Gamma/dT_s)]$, which can imply substantial apparent super or sub-CC scaling. For a moist adiabatic column where Γ decreases with warming, we expect Q to scale roughly $2.5\%\,\mathrm{K}^{-1}$ greater than the saturation vapor pressure at the ambient T_s.

We analyzed the spatial structure of temperature and water vapor changes in six perturbation experiments with an idealized aquaplanet slab ocean GCM. We studied the warming and moistening associated with a doubling of CO_2 and compared it to the combined effects of CO_2 and imposed ocean heat uptake, in analogy with the long transient response to radiative forcing in coupled GCMs. Following Rose et al. (2014) we compared heat uptake patterns localized to the high latitudes and the tropics, and studied the response to the uptake in isolation as well as in combination with CO_2 radiative forcing. Finally we studied the response to an imposed increase in equator-to-pole ocean heat transport following the method of Rose and Ferreira (2013).

Our simulations span a wide range of different spatial structures of surface temperature and lapse rate change, and consequently sample a wide variety of different water vapor scalings. Here $\delta Q_{\mathrm{global}}$ ranges between 3.6% and $11.0\%\,\mathrm{K}^{-1}$. All of these wide-ranging values of $\delta Q_{\mathrm{global}}$ are essentially consistent with the Clausius–Clapeyron relation; changes in relative humidity are very minor in most cases. Consistent with previous studies, we find that this diagnostic is strongly constrained by the degree of polar amplification of surface temperature change. New in our study, we are able to quantify the effect of changing lapse rates, and find that these are also wide ranging in our ensemble of simulations. The lapse rate contribution is largest in those simulations with enhanced midtropospheric warming relative to the surface; these include our tropically forced heat uptake case (q_T) and our combined forcing case with high-latitude heat uptake ($2 \times CO_2 + q_H$).

This combined forcing case has special significance because OHU is typically localized to the subpolar oceans in coupled GCM simulations of global warming (Winton et al. 2010; Bitz et al. 2012; Rose et al. 2014)—and presumably in nature as well. Comparing our $2 \times CO_2$ and $2 \times CO_2 + q_H$ cases is thus analogous to equilibrium versus transient climate changes. Consistent with previous studies, the "equilibrium" case exhibits smaller $\delta Q_{\mathrm{global}}$ than the "transient" case. This difference is not solely due to surface warming and polar amplification patterns; the lapse rate contribution is large in our transient case ($+2.1\%\,\mathrm{K}^{-1}$). The combination of greenhouse radiative forcing and subpolar OHU produces proportionally more warming of the lower to midtroposphere and less at the surface than radiative forcing alone. This result cannot be understood as a strictly local effect of OHU; it involves a global, dynamically mediated atmospheric response, and may have some interesting implications for other aspects of the hydrological cycle under transient and equilibrium climate change.

Our imposed OHU forcings mimic coupled atmosphere–ocean processes that occur in nature and in fully coupled models, but they are highly idealized. One could imagine other spatially localized forcing agents (e.g., perturbations to cloud properties, surface albedo, or aerosols) that generate surface temperature patterns similar to Fig. 4b. Would Q scale the same way in such scenarios? Or is the response particular to OHU? The answer depends on whether or not RH and lapse rate changes are strongly constrained by surface temperature, independently of the forcing mechanism. This is not true in general—climate response, including lapse rates, depend not just on latitude of forcing but also on its altitude and physical nature (Hansen et al. 1997). In a recent example, Kim et al. (2015) showed that lapse rate changes in response to subtropical black

carbon (an absorbing aerosol) depend strongly on its altitude. On the other hand, we speculate that any forcing mechanism operating primarily through changes to sea surface shortwave absorption ought to behave similarly to OHU, since the atmospheric response is mediated by surface heat fluxes regardless of the ultimate driver. Examples might include optical properties of low-level marine clouds (Latham et al. 2008) or sea ice (Goldenson et al. 2012).

While our GCM is relatively comprehensive, our calculations use idealized aquaplanet boundary conditions. We chose this experimental framework for simplicity and to follow up on the heat uptake study by Rose et al. (2014). We acknowledge some limitations of the analogy between the aquaplanet and Earth. It is possible that by excluding land surfaces we are systematically underestimating the importance of RH changes, since boundary layer RH is less tightly constrained over land than ocean. O'Gorman and Muller (2010) found scalings of surface relative humidity changes about 1 to 2% K^{-1} lower over land than neighboring ocean regions. We also find that our transient and equilibrium values for δQ_{global} are both larger than those reported by Back et al. (2013) for "fast" and "slow" warming in a coupled historical simulation. Now that we have established a diagnostic framework for evaluating RH and lapse rate contributions, it would be interesting to repeat similar experiments in a more Earth-like model setup.

Another caveat concerns the importance of RH changes. Our study is limited to understanding the changes in precipitable water. To this end we have plotted RH changes weighted by the background specific humidity. This weighting deemphasizes the *radiatively* important upper-tropospheric RH changes, which we have not discussed here. In fact the water vapor feedback differs substantially across this suite of simulations, with implications for understanding the efficacy of ocean heat uptake (Rose et al. 2014, and ongoing studies).

Our local decomposition in (14) treats surface temperature and lapse rate changes as separate contributions to the changes in Q, in the tradition of radiative feedback analysis. In reality the horizontal and vertical spatial patterns of temperature change are not physically independent, but are coupled together through baroclinic eddy dynamics. Frierson (2008) has shown, for example, a strong relationship between vertical and horizontal gradients of equivalent potential temperature across a wide range of climates in aquaplanet simulations. This suggests that the same eddies whose moist energy transport is partly responsible for setting the degree of surface polar amplification in different forcing scenarios (Rose et al. 2014) are also responsible for determining lapse rate changes, and thus the water vapor storage capacity of the atmosphere. Future work will focus on linking these dynamical constraints to the local column view of Q espoused in this paper.

To summarize our main conclusions, a wide variety of different scalings of precipitable water are found in simulations of climate change driven by combinations of greenhouse gases and ocean heat fluxes. These scalings are all essentially consistent with the Clausius–Clapeyron relation. The diversity is explained first by spatial patterns of surface temperature change, followed closely by the vertical structure of temperature change, with relative humidity changes playing only a minor small role. We have shown that heat fluxes in and out of the ocean exert a strong influence on thermal structure of the atmosphere, with important consequences (through the CC relation) for the ability of the atmosphere to hold water vapor. Thus, we should expect Q to vary widely on different time scales, both in nature and in coupled simulations, as the spatial pattern of ocean heat fluxes evolves. We have also shown there are many inconsistencies between the local and global perspectives. Methodological care is thus required in any future discussion of the scaling of atmospheric water vapor under climate change.

Acknowledgments. NCEP Reanalysis 2 data were provided by the NOAA/OAR/ESRL PSD, Boulder, Colorado, from their website (http://www.esrl.noaa.gov/psd/). BR thanks Cecilia Bitz and Larissa Back for helpful discussions during the early stages of this work. We also thank two anonymous reviewers for their thoughtful comments. This work was supported by NSF Award AGS-1455071.

APPENDIX A

Analytical Solutions for Uniform Lapse Rate and Relative Humidity

Here we explicitly evaluate the integral in (1) for precipitable water in a column with vertically uniform relative humidity and lapse rate. The specific humidity is related to vapor pressure e through

$$q = \varepsilon \frac{e}{p - (1 - \varepsilon)e}, \tag{A1}$$

where $\varepsilon = R_d/R_v$ is the ratio of gas constants for dry air and water vapor (e.g., Rogers and Yau 1989). Assuming a

relatively dilute mixture of dry air and water vapor, (A1) simplifies to

$$q \approx r\varepsilon \frac{e_s(T)}{p}. \tag{A2}$$

To a good approximation (ignoring the weak temperature dependence of the latent heat of vaporization), the CC relation in (2) can be integrated to give

$$e_s(T) \approx A \exp\left(-\frac{L}{R_v T}\right), \tag{A3}$$

where $A = 2.53 \times 10^9$ hPa (Rogers and Yau 1989). We note that for a hydrostatic, ideal gas atmosphere with vertically uniform lapse rate Γ,

$$\frac{T(p)}{T_s} = \left(\frac{p}{p_0}\right)^{\gamma}, \tag{A4}$$

where the exponent γ is a nondimensional measure of the lapse rate:

$$\gamma = \kappa \frac{\Gamma}{\Gamma_d} = \frac{R_d \Gamma}{g}, \tag{A5}$$

where $\kappa = R_d/c_p$ and $\Gamma_d = g/c_p$ is the dry adiabatic lapse rate. Plugging (A2), (A3), and (A4) into (1) gives

$$Q = \frac{r\varepsilon A}{g} \int_0^{p_0} \frac{1}{p} \exp\left[-\frac{L}{R_v T_s}\left(\frac{p}{p_0}\right)^{-\gamma}\right] dp, \tag{A6}$$

where we bring r out of the integral under the assumption of vertically uniform RH.

The integral can be put in standard form through the change of variables:

$$t = l\left(\frac{p}{p_0}\right)^{-\gamma} \quad l = \frac{L}{R_v T_s}, \tag{A7}$$

so that

$$\frac{dp}{p} = -\frac{1}{\gamma}\frac{dt}{t} \tag{A8}$$

and the integral can be written as

$$Q = \frac{r\varepsilon A}{g\gamma} \int_l^{\infty} \frac{e^{-t}}{t} dt = -\frac{r\varepsilon A}{g\gamma} \mathrm{Ei}(-l) \tag{A9}$$

with Ei as the exponential integral function [Olver et al. (2010), see their Eq. (6.2.6)], which has the property $[d\mathrm{Ei}(x)]/dx = e^x/x$. Substituting (A7), (A5), and $\varepsilon = R_d/R_v$ into (A9) then gives

$$Q = -\frac{rA}{R_v \Gamma} \mathrm{Ei}\left(\frac{-L}{R_v T_s}\right), \tag{A10}$$

which notably says Q depends on Γ^{-1}.

Taking the derivative of (A10) with respect to T_s and dividing through by Q gives the fractional rate of change:

$$\frac{1}{Q}\frac{dQ}{dT_s} = -\frac{1}{T_s}\frac{\exp(-l)}{\mathrm{Ei}(-l)} - \frac{1}{\Gamma}\frac{d\Gamma}{dT_s} + \frac{1}{r}\frac{dr}{dT_s} \tag{A11}$$

and it can be shown that, for large l,

$$-\frac{\exp(-l)}{\mathrm{Ei}(-l)} \approx l, \tag{A12}$$

which yields the result in (16).

APPENDIX B

Effects of Temperature Dependence of the Latent Heat on Saturation Vapor Pressure

The latent heat L in the CC relation in (2) is not constant. For $T > 0$°C, or in the presence of supercooled water, $L = L_v$, the latent heat of vaporization. The variable L_v is a weakly decreasing function of temperature, varying by about 6% between −30° and +30°C (Rogers and Yau 1989). For $T < 0$°C the vapor phase may be in equilibrium with ice crystals; in this case the appropriate value of L is the latent heat of sublimation L_s, with $L_s > L_v$.

The default method for computing e_s in CAM includes a linear interpolation between saturation with respect to water at 0°C and saturation with respect to ice at −20°C (assuming no supercooled water for $T < -20$°C). In the main text, we compute e_s and q_{sat} by these same formulas. Here we briefly compare these values to several other commonly used implementations of the CC relation:

1) CAM default: saturation formulas from Goff and Gratch (1946), with linear transition between water and ice saturation.
2) A modified Tetens's formula with quadratic transition between water and ice saturation (with thresholds at 0° and −23°C). Used operationally in ECMWF models, details in Simmons et al. (1999), also used by Boos (2012).
3) Empirical formula from Bolton (1980); no explicit transition between water and ice saturation.
4) Constant L, taking L_v at 0°C.

Figure B1 (left panel) shows $\alpha = (1/e_s)(de_s/dT)$ as a function of temperature. All methods agree at 0°C,

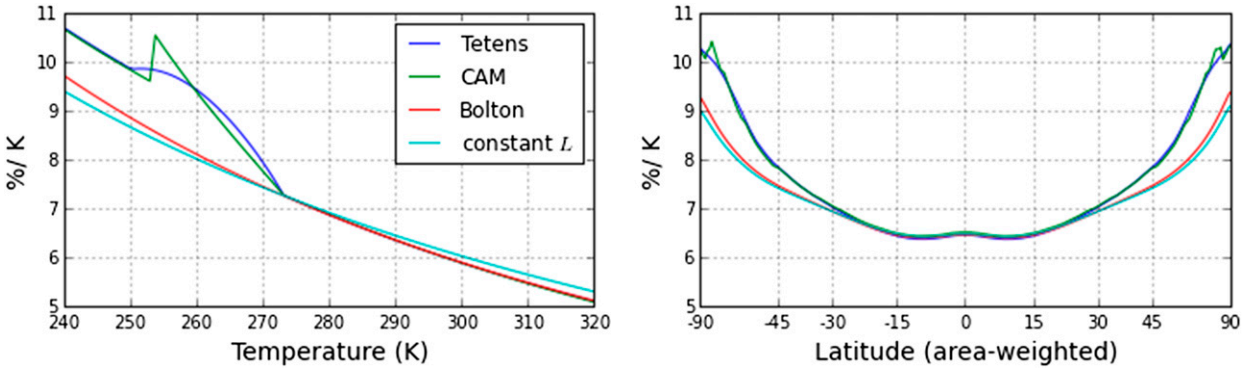

FIG. B1. Comparing four different versions of the Clausius–Clapeyron relation. (left) $\alpha(T)$ is the fractional rate of change in saturation vapor pressure. (right) $\langle\alpha(T)\rangle$ is the uniform warming contribution to column water vapor changes in our GCM control climate.

where $\alpha = 7.26\%\ \mathrm{K}^{-1}$, and differences at warmer temperatures are very small. The important differences occur for colder temperatures where assumptions about ice versus water saturation come into play. The methods that do not account for saturation with respect to ice underestimate α by about $1.5\%\ \mathrm{K}^{-1}$ at $-15°\mathrm{C}$. The CAM method gives a discontinuity in α at the threshold temperature $-20°\mathrm{C}$ because of the linear interpolation scheme for e_s.

The right panel of Fig. B1 shows the uniform warming contribution to fractional changes in Q, $\delta Q_{T_s} = \langle(1/q_{\mathrm{sat}})(dq_{\mathrm{sat}}/dT)\rangle$ computed from our aquaplanet control simulation. The estimates of δQ_{T_s} differ mainly at high latitudes where temperatures are cold. Methods that do not account for saturation with respect to ice underestimate δQ_{T_s} by about $1.5\%\ \mathrm{K}^{-1}$ at 70° latitude.

Table B1 shows the corresponding global averages (uniform contributions to $\overline{\delta Q_{\mathrm{hybrid}}}$). These vary by as much as $0.6\%\ \mathrm{K}^{-1}$ for each experiment depending on which method is used to calculate $\langle\alpha\rangle$. The spread is largest in the experiments with the greatest polar amplification (q_H, OHT) and weakest in the experiments with tropical amplification (q_T, $2\times\mathrm{CO_2} + q_H$) due to the weighting of the global mean by the local temperature amplification factor τ.

Do these differences matter? Not for the global diagnostics $\delta Q_{\mathrm{global}}$ and its decomposition. The analogous results to Table B1 for $\delta Q_{\mathrm{global}}$ is not shown because the differences are $<= 0.1\%\ \mathrm{K}^{-1}$ in all cases, due to the strong weighting of this diagnostic to the warm tropics where the differences between the CC methods are negligible. However, accurate calculation of the decomposition of $\delta Q_{\mathrm{local}}$ at higher latitudes (and its projection onto the global mean $\overline{\delta Q_{\mathrm{hybrid}}}$) does depend on the CC method. By adopting the same version of the CC relation used in the GCM for our diagnostic calculations, we keep the residuals in Tables 1 and 2 quite small. Using a less-accurate version of the CC relation would in some cases increase these residual errors to the same order as the lapse rate contribution, rendering our decomposition less meaningful.

The residual in Table 1 is still relatively large for q_H ($-0.4\%\ \mathrm{K}^{-1}$). This is likely due to nonlinear effects of temperature fluctuations not resolved in the time-mean model output. The errors show up most strongly in q_H because of large temperature changes at high latitudes in this experiment.

TABLE B1. Global mean of $\langle\alpha(T)\rangle$, the uniform warming contributions to the *local* fractional changes in column water vapor, calculated with four different versions of the Clausius–Clapeyron relation. The equivalent table for contributions to *global* fractional changes in Q is not shown because the differences are $<= 0.1\%\ \mathrm{K}^{-1}$ in all cases.

	$2\times\mathrm{CO_2}$	$2\times\mathrm{CO_2} + q_H$	$2\times\mathrm{CO_2} + q_T$	q_H only	q_T only	OHT ($N = 2$)
Tetens	7.7	7.3	7.7	8.3	7.2	8.1
CAM	7.7	7.3	7.8	8.3	7.2	8.1
Bolton	7.3	7.0	7.3	7.7	7.0	7.6
Constant L	7.2	7.0	7.3	7.6	6.9	7.5

REFERENCES

Back, L., K. Russ, Z. Liu, K. Inoue, J. Zhang, and B. L. Otto-Bliesner, 2013: Global hydrological cycle response to rapid and slow global warming. *J. Climate*, **26**, 8781–8786, doi:10.1175/JCLI-D-13-00118.1.

Barreiro, M., A. Cherchi, and S. Masina, 2011: Climate sensitivity to changes in ocean heat transport. *J. Climate*, **24**, 5015–5030, doi:10.1175/JCLI-D-10-05029.1.

Bitz, C., K. Shell, P. Gent, D. Bailey, G. Danabasoglu, K. Armour, M. Holland, and J. Kiehl, 2012: Climate sensitivity of the Community Climate System Model, version 4. *J. Climate*, **25**, 3053–3070, doi:10.1175/JCLI-D-11-00290.1.

Blackburn, M., and B. J. Hoskins, 2013: Context and aims of the aqua-planet experiment. *J. Meteor. Soc. Japan*, **91A**, 1–15, doi:10.2151/jmsj.2013-A01.

Bolton, D., 1980: The computation of equivalent potential temperature. *Mon. Wea. Rev.*, **108**, 1046–1053, doi:10.1175/1520-0493(1980)108<1046:TCOEPT>2.0.CO;2.

Boos, W. R., 2012: Thermodynamic scaling of the hydrological cycle of the last glacial maximum. *J. Climate*, **25**, 992–1006, doi:10.1175/JCLI-D-11-00010.1.

Crook, J. A., P. M. Forster, and N. Stuber, 2011: Spatial patterns of modeled climate feedback and contributions to temperature response and polar amplification. *J. Climate*, **24**, 3575–3592, doi:10.1175/2011JCLI3863.1.

Frierson, D. M. W., 2008: Midlatitude static stability in simple and comprehensive general circulation models. *J. Atmos. Sci.*, **65**, 1049–1062, doi:10.1175/2007JAS2373.1.

Goff, J. A., and S. Gratch, 1946: Low-pressure properties of water from −160° to 212°F. *Trans. Amer. Soc. Heat. Vent. Eng.*, **51**, 125–164.

Goldenson, N., S. J. Doherty, C. M. Bitz, M. M. Holland, B. Light, and A. J. Conley, 2012: Arctic climate response to forcing from light-absorbing particles in snow and sea ice in CESM. *Atmos. Chem. Phys.*, **12**, 7903–7920, doi:10.5194/acp-12-7903-2012.

Gregory, J. M., and Coauthors, 2004: A new method for diagnosing radiative forcing and climate sensitivity. *Geophys. Res. Lett.*, **31**, L03205, doi:10.1029/2003GL018747.

Hansen, J., M. Sato, and R. Ruedy, 1997: Radiative forcing and climate response. *J. Geophys. Res.*, **102**, 6831–6864, doi:10.1029/96JD03436.

Held, I. M., and B. J. Soden, 2006: Robust responses of the hydrological cycle to global warming. *J. Climate*, **19**, 5686–5699, doi:10.1175/JCLI3990.1.

Herweijer, C., R. Seager, M. Winton, and A. Clement, 2005: Why ocean heat transport warms the global mean climate. *Tellus*, **57A**, 662–675, doi:10.1111/j.1600-0870.2005.00121.x.

Kanamitsu, M., W. Ebisuzaki, J. Woollen, S.-K. Yang, J. J. Hnilo, M. Fiorino, and G. L. Potter, 2002: NCEP–DOE AMIP-II Reanalysis (R-2). *Bull. Amer. Meteor. Soc.*, **83**, 1631–1643, doi:10.1175/BAMS-83-11-1631.

Kim, H., S. M. Kang, Y.-T. Hwang, and Y.-M. Yang, 2015: Sensitivity of the climate response to the altitude of black carbon in the northern subtropics in an aquaplanet GCM. *J. Climate*, **28**, 6351–6359, doi:10.1175/JCLI-D-15-0037.1.

Koll, D. D. B., and D. S. Abbot, 2013: Why tropical sea surface temperature is insensitive to ocean heat transport changes. *J. Climate*, **26**, 6742–6749, doi:10.1175/JCLI-D-13-00192.1.

Latham, J., and Coauthors, 2008: Global temperature stabilization via controlled albedo enhancement of low-level maritime clouds. *Philos. Trans. Roy. Soc. London*, **A366**, 3969–3987, doi:10.1098/rsta.2008.0137.

Lee, M.-I., M. J. Suarez, I.-S. Kang, I. M. Held, and D. Kim, 2008: A moist benchmark calculation for atmospheric general circulation models. *J. Climate*, **21**, 4934–4954, doi:10.1175/2008JCLI1891.1.

Lorenz, D. J., and E. T. DeWeaver, 2007: The response of the extratropical hydrological cycle to global warming. *J. Climate*, **20**, 3470–3484, doi:10.1175/JCLI4192.1.

Neale, R. B., and B. J. Hoskins, 2000: A standard test for AGCMs including their physical parameterizations: I: The proposal. *Atmos. Sci. Lett.*, **1**, 101–107, doi:10.1006/asle.2000.0022.

——, J. Richter, S. Park, P. H. Lauritzen, S. J. Vavrus, P. J. Rasch, and M. Zhang, 2013: The mean climate of the Community Atmosphere Model (CAM4) in forced SST and fully coupled experiments. *J. Climate*, **26**, 5150–5168, doi:10.1175/JCLI-D-12-00236.1.

O'Gorman, P. A., and C. J. Muller, 2010: How closely do changes in surface and column water vapor follow Clausius–Clapeyron scaling in climate change simulations? *Environ. Res. Lett.*, **5**, 025207, doi:10.1088/1748-9326/5/2/025207.

Olver, F. W. J., D. W. Lozier, R. F. Boisvert, and C. W. Clark, Eds., 2010: *NIST Handbook of Mathematical Functions.* Cambridge University Press, 968 pp.

Pierrehumbert, R. T., 2010: *Principles of Planetary Climate.* Cambridge University Press, 680 pp.

Rogers, R., and M. Yau, 1989: *A Short Course in Cloud Physics.* 3rd ed. International Series in Natural Philosophy, Vol. 113, Pergamon, 304 pp.

Rose, B. E. J., and D. Ferreira, 2013: Ocean heat transport and water vapor greenhouse in a warm equable climate: A new look at the low gradient paradox. *J. Climate*, **26**, 2117–2136, doi:10.1175/JCLI-D-11-00547.1.

——, K. C. Armour, D. S. Battisti, N. Feldl, and D. D. B. Koll, 2014: The dependence of transient climate sensitivity and radiative feedbacks on the spatial pattern of ocean heat uptake. *Geophys. Res. Lett.*, **41**, 1071–1078, doi:10.1002/2013GL058955.

Simmons, A. J., A. Untch, C. Jakob, P. Kållberg, and P. Undén, 1999: Stratospheric water vapour and tropical tropopause temperatures in ECMWF analyses and multi-year simulations. *Quart. J. Roy. Meteor. Soc.*, **125**, 353–386, doi:10.1002/qj.49712555318.

Stone, P. H., 1978: Baroclinic adjustment. *J. Atmos. Sci.*, **35**, 561–571, doi:10.1175/1520-0469(1978)035<0561:BA>2.0.CO;2.

Winton, M., K. Takahashi, and I. M. Held, 2010: Importance of ocean heat uptake efficacy to transient climate change. *J. Climate*, **23**, 2333–2344, doi:10.1175/2009JCLI3139.1.